

See discussions, stats, and author profiles for this publication at: <https://www.researchgate.net/publication/259077770>

Photoelectrochemical Transients for Chlorine/Hypochlorite Formation at "Roll-On" Nano-WO₃ Film Electrodes

DATASET in THE JOURNAL OF PHYSICAL CHEMISTRY C · DECEMBER 2013

Impact Factor: 4.77 · DOI: 10.1021/jp400962t

CITATIONS

11

READS

63

4 AUTHORS, INCLUDING:



Ibrahim A.I. Hassan

South Valley University

5 PUBLICATIONS 12 CITATIONS

[SEE PROFILE](#)

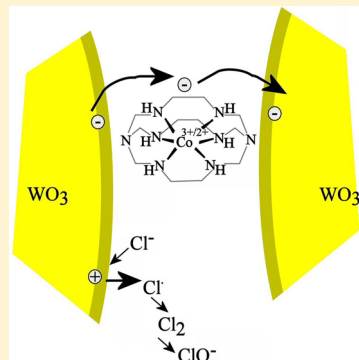
Photoelectrochemical Transients for Chlorine/Hypochlorite Formation at “Roll-On” Nano-WO₃ Film Electrodes

Safeer Ahmed,^{†,‡} Ibrahim A.I. Hassan,[†] Hayley Roy,[†] and Frank Marken*,[†]

[†]Department of Chemistry, University of Bath, Bath BA2 7AY, United Kingdom

[‡]Department of Chemistry, Quaid-i-Azam University, 45320 Islamabad, Pakistan

ABSTRACT: Commercial nano-WO₃ (10–100 nm average particle size) is dispersed in *n*-hexanol and applied to tin-doped indium oxide (ITO) substrates in a simple “roll-on” process. As-deposited and annealed (500 °C) films are compared and shown to be photoactive for the formation of hypochlorite in neutral aqueous NaCl (e.g., seawater). Annealing at 500 °C in air improves photocurrents most likely due to improved interparticle charge transport (e.g., removal of hydration or *n*-hexanol surface layers). In phototransients (interpreted here in the limiting case of a weakly associated nanoparticle aggregate as opposed to the limiting case of a single-crystal semiconductor), evidence for the presence of both holes (as O(-I), fast moving) and electrons (as W(V), slow moving) is obtained in particular in as-deposited films. Bipotentiostat experiments reveal the presence of chlorine as a reaction intermediate close to the photoanode when immersed in 3 M NaCl. A “molecular conduit” effect with adsorbed Co(II/III) sepulchrone is observed to significantly enhance the photocurrents at as-deposited electrodes (but not at annealed electrodes).



1. INTRODUCTION

Aggregates and films of semiconductor nanoparticles provide extremely high surface area with improved contact between solid and liquid phase, for example, for photoelectrolytic devices. In the limiting case of weakly interacting nanoparticle aggregates, the properties of these assembled surfaces may be considered similar to “molecular assemblies”¹ with slow interparticle hopping of charge carriers. In contrast to this, annealing and sintering leads to a stronger interaction between particles and a more continuous solid phase “backbone” with properties of aggregates approaching those of the limiting case of a flat surface (or single crystal semiconductor). The transition from weakly interacting to annealed aggregate films is of wider interest and investigated here for nanoparticulate tungsten trioxide.

Tungsten trioxide WO₃ is one of the pigments with promise for photoelectrochemical energy harvesting.^{2,3} WO₃ as a relatively low cost and as a sustainable material could be applied in a range of photoelectrolysis processes. Applications in wastewater remediation have been proposed.⁴ Efficient photoelectrochemical processes in particular with nano-WO₃ are possible.⁵ The formation of WO₃ films as electrodes has previously been achieved by sol–gel methods,⁶ electrodeposition,⁷ vacuum coating methods,⁸ and industrial screen-printing or doctor blading methods.⁹ The role of the organic dispersion reagent during doctor blading on WO₃ properties has been studied¹⁰ and recombination dynamics for electrons and holes have been investigated by transient adsorption spectroscopy.¹¹

Tungsten trioxide in bulk is an n-type semiconductor with a band gap of approximately 2.7 eV,¹² absorbing light in the blue

visible region and emitting to give the characteristic yellow appearance of tungsten in a 6+ oxidation state. Nanostructured tungsten oxide is particularly relevant in photochromic devices due to color changes in oxidation state between W(V) (blue) and W(VI) (yellow).¹³ Tungsten oxide has been observed to have different crystal structures on changing temperature.¹⁴ For commercial powders, the final high temperature (>900 °C) crystal lattice has been shown to be tetragonal.¹⁵ Nano-WO₃ may also occur in amorphous form,¹⁶ in particular, at lower temperature. Tungsten trioxide has been employed in photo-oxidation of water to produce oxygen¹⁷ and other products.¹⁸

WO₃ film properties for water splitting applications have been reviewed and compared to other oxide photoanode materials.¹⁹ In 1 M H₂SO₄ solution, WO₃ is reported to possess a photoanodic onset potential of about 0.16 V versus SCE. The light yellow color is consistent with an absorption maximum at about 400 nm. Oxygen or chlorine evolution in aqueous media under visible light (AM1.5) irradiation has been shown to produce photocurrents of typically about 3 mA cm⁻².²⁰ For meso-structured films of about 2.5 μm thickness (prepared via sol–gel methods) incident photon to current efficiency (IPCE) values of close to 100% as well as current doubling phenomena have been reported.^{21,22}

In this report, a simple “roll-on” process (from *n*-hexanol suspension) for the deposition of a commercial amorphous WO₃ nanopowder is used to fabricate simple weakly associated photoactive films on tin-doped indium oxide (ITO). An anneal

Received: January 28, 2013

Revised: March 6, 2013

Published: March 13, 2013

process at 500 °C in air is shown to considerably enhance photoelectrochemical responses (transients and photostationary currents). In neutral aqueous chloride containing electrolyte media formation of chlorine/hypochlorite is demonstrated with substantial photocurrent increase even beyond 0.5 M NaCl (equivalent to seawater). In weakly associated films, photoelectrochemical transients are consistent (at least qualitatively) with two types of mobile photoinduced charge carriers: fast holes (chemically O(-I) radicals) and slow electrons (chemically W(V) surface sites). A “molecular conduit” effect for the Co(sep)³⁺ redox mediator is shown to enhance photocurrents at “as-deposited films” (but not at annealed films) by 1 order of magnitude, probably by enhancing interparticle electron mobility. Mechanistic implications are discussed.

2. EXPERIMENTAL SECTION

2.1. Chemical Reagents. Reagents used were 99.9% tungsten trioxide nanopowder (amorphous, A.P.S. <100 nm) purchased from American Elements (California, U.S.A.), NaCl, and *n*-hexanol purchased from Sigma-Aldrich. Aqueous solutions were prepared with deionized and filtered water taken from a Thermo Scientific water purification system (Barnstead Nanopure) with not less than 18.2 MΩ·cm resistivity.

2.2. Instrumentation. Electrochemical measurements were performed using either a μAutolab Type II potentiostat system or a PGSTAT30 (Ecochemie, NL) with Autolab GPES software or for impedance experiments an IviumCompactstat (Ivium Technologies, NL). The electrodes used for electrochemical experiments were a platinum wire counter electrode and a potassium chloride saturated calomel (SCE) reference electrode. The working electrodes were made from tin-doped indium oxide (ITO, Image Optics Components, Basildon, Essex) coated glass, cut to give 1 × 3 cm² electrodes (washed with ethanol and distilled water followed by heat treatment in a 500 °C furnace in air for 30 min, re-equilibrated to room temperature) with 1 cm² exposed area. All electrochemical experiments were performed in a Faraday cage with a high power blue LED ($\lambda = 405$ nm, M405L2 UV LED, Thorlabs) together with LED driver (T-Cube LED driver, Thorlabs) and a DDS Function/Arbitrary TG4001 Generator to set pulse frequency and intensity. Photocurrent spectra (IPCE data) were recorded both for EE (electrolyte entry) and SE (substrate entry) illumination. The light intensity was calibrated using a silicon photodiode. The photocurrent was plotted as a function of incident light with λ ranging from 350 to 500 nm in steps of 10 nm. The chopper frequency was set at 3 Hz. The apparatus was based on a Stanford Research Systems SR830 lock in amplifier, SR540 chopper controller, a homemade potentiostat, a 75 W xenon lamp powered by an Bentham 650 power supply, and a monochromator controller PMC3B of Bentham Instruments Ltd. U.K. Reflectance UV/vis spectra were obtained on a Perkin-Elmer Lambda 35 with integration sphere attachment. Scanning electron microscopy (SEM) images were obtained using a JEOL JSM6301F microscope. A Bruker D8 Advance powderdiffractometer with Cu K α radiation (1.5418 Å) was used for powder XRD. Numerical simulation was performed in a Matlab 7.11.0 (R2012b) environment.

2.3. “Roll-On” Procedure for Making Electrodes. WO₃ nanopowder was deposited onto ITO electrodes using 30 mg/mL nano-WO₃ in *n*-hexanol, which was suspended by

sonication for 30 min before deposition. The deposition was carried out by employing a drawing roller (hard rubber lino printing roller, see Figure 1A) on a hard substrate to evenly

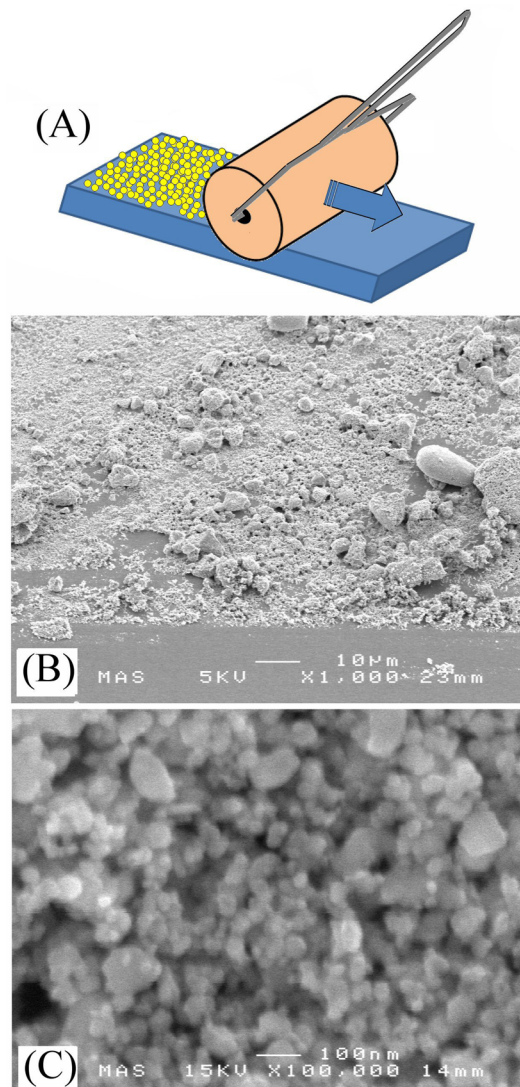


Figure 1. Film deposition setup (A) roller with sample and SEM images of the annealed sample in (B) low and (C) high magnification showing amorphous nano-WO₃ deposited on ITO.

distribute the nanoparticles. The WO₃ suspension was rolled onto the ITO substrate. The WO₃ deposited ITO glass slide was then dried in air for 2 h. The process was repeated to increase the thickness of the WO₃ nanoparticle film.

From SEM imaging it is apparent (see Figure 1B,C) that nanoparticles of 10 to 100 nm average particle size are deposited in aggregates of up to 10 μm. The thickness of the film is uneven but within 1 to 10 μm. Similar SEM images obtained for as-deposited WO₃ films show the same particle size distribution (substantial sintering only occurs >500 °C²³) but lower electrical conductivity causes blurring of the images. Both as-deposited and annealed WO₃ samples are X-ray amorphous.

3. RESULTS AND DISCUSSION

3.1. Photoelectrochemical Hypochlorite Formation I: Photovoltaometry.

The photoelectrochemical reaction of

chloride at WO_3 anodes has been reported previously and shown to yield chlorine in acidic media or “active chlorine” from seawater,¹⁸ which is important, for example, in disinfection and cleaning purposes. At pH > 7.5 chlorine is readily converted into hypochlorite with lower disinfection ability but better storage and handling characteristics.²⁴ Here experiments are carried out in chloride containing aqueous media under neutral conditions and with a “simple” WO_3 nanopowder film electrode.

Typical cyclic voltammograms for the “as-deposited” WO_3 film electrode on ITO are shown in Figure 2B. In the first

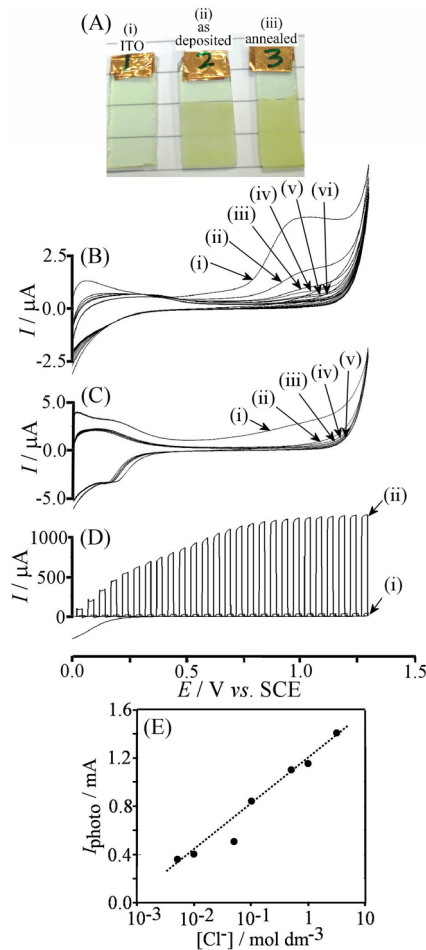
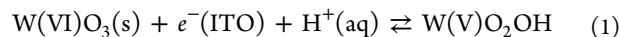


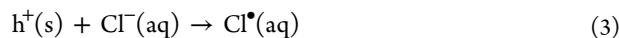
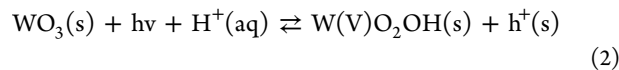
Figure 2. (A) Photograph of (i) a bare ITO electrode, (ii) a “as-deposited”, and (iii) an “annealed” WO_3 thin film electrode. (B) Cyclic voltammograms (scan rate 10 mV s⁻¹, (i)–(vi) indicate consecutive potential cycles for as-deposited WO_3 film electrode immersed in aqueous 3 M NaCl. (C) As before, but using an annealed WO_3 film electrode. (D) Photocurrent transients (scan rate 10 mV s⁻¹, light pulses 2.5 on 2.5 s off, $\lambda = 405$ nm) for (i) as-deposited and (ii) annealed nano- WO_3 film electrodes immersed in 3 M NaCl. (E) Plot of the photocurrent at 0.7 V vs SCE vs NaCl concentration.

potential cycles, a characteristic peak at about 1.0 V versus SCE is indicative of oxidation of W(V) surface states (visible as green coloration of the nano- WO_3 powder). This irreversible response rapidly decays to leave a chemically reversible reduction/oxidation signal at about 0.2 V versus SCE. This is assigned here tentatively to the onset of W(V) surface state formation (eq 1, compare to the prevailing model for electrochromic responses²⁵).



The nano- WO_3 film, when annealed, has a pale yellow appearance (see Figure 2A) and the oxidation feature at 1.0 V versus SCE is insignificant. However, the reversible reduction at 0.2 V versus SCE (see Figure 2C, eq 1) is now peak-shaped and therefore better defined. This voltammetric response is also significantly higher in current presumably due to a better conductivity for charge carriers in the annealed WO_3 material. The onset of direct chloride oxidation in 3 M NaCl is observed at about 1.3 V versus SCE.

When light pulses are applied during cyclic voltammetry (blue LED, $\lambda = 405$ nm, Figure 2D) characteristic anodic current pulses are observed. These current pulses are associated with photo-oxidation of a solution component, here chloride. The effect of the chloride concentration on the photocurrent is shown in Figure 2E. A logarithmic dependency is linked to a competitive process, here the formation of “active chlorine” versus recombination of charge carriers (direct electron–hole recombination and/or indirect when solution chlorine interacts with the electrode). The process is summarized in eqs 2–4 assuming formation of a W(V) “trap state” and a “hole” $\text{h}^+(\text{s})$ (chemically probably a O(-I) state) at the WO_3 /solution interface (consistent with the density of states plots¹¹).



The effect of nano- WO_3 film thickness was investigated and additional layers of WO_3 did lead to a further increase in photocurrent (up to ca. 1.5 mA for annealed films), but also additional resistivity was introduced when films are applied too thick. A comparison of substrate exposure (SE) versus electrolyte exposure (EE) clearly indicated that the nano- WO_3 films employed here are relatively nonuniform and optically nontransparent and therefore require illumination from the substrate.

The UV/vis reflectance spectrum shows a transition (similar for as-deposited and annealed film samples) with onset at about 480 nm (see Figure 3A). This is in agreement with literature reports²⁶ and consistent with IPCE (incident photon to current conversion efficiency) measurements (see Figure 3B) where the improved photocurrent yield in SE configuration is clearly seen.

The appearance of the IPCE data agrees with literature reports³ and for a range of annealed samples studied here up to 15% IPCE were observed. This value is low, likely due to the relatively high chopping frequency (here 3 Hz) and is therefore not an absolute measure of the practical performance of these WO_3 films.

3.2. Photoelectrochemical Hypochlorite Formation II: Product Detection. The formation of chlorine and hypochlorite is of considerable importance in disinfection and water treatment. The photochlorination in aqueous chloride based on TiO_2 electrodes²⁷ and based on WO_3 electrodes²⁸ has been reported. The product distribution is pH-dependent and chlorine is stable in solution only in mildly acidic media (pH < 7.5), whereas hypochlorite as a less volatile form of active chlorine dominates at neutral and mildly alkaline conditions. In order to explore the mechanism of the photoelectrochemical hypochlorite formation a “generator–collector electrode”

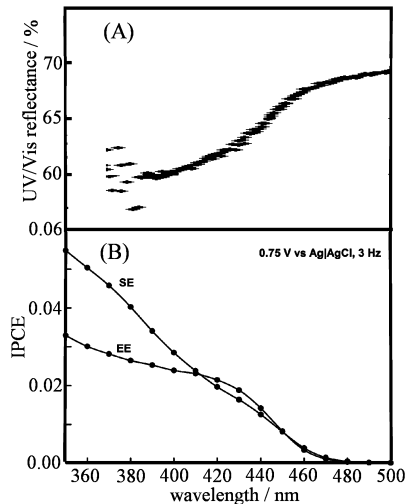


Figure 3. (A) Reflectance UV/vis spectrum for an annealed WO_3 film electrode. (B) IPCE data (at 3 Hz, SE = substrate exposure, EE = electrolyte exposure) for an annealed WO_3 film electrode immersed in aqueous 3 M NaCl at 3 Hz frequency and 0.75 V vs Ag/AgCl applied potential.

method can be employed. Here, a 50 μm diameter platinum wire with Teflon coating is employed with the end exposed to the solution phase in the immediate vicinity of the WO_3 photoanode (see drawing in Figure 4A).

The “as-deposited” electrode develops only low levels of photoproducts and therefore the “annealed” electrode is investigated. Figure 4B shows photoanodic current transients in 3 M NaCl. The product detection at the Pt microelectrode is shown at three applied potentials for 0.3, 0.7, and 1.0 V versus SCE (see Figure 4C–E). It can be observed that each photoanodic current pulse at the generator electrode is associated with a reduction current at the Pt microelectrode. The magnitude of this reduction current is dependent on the applied collector potential with about 50, about 30, and about 20 nA at 0.3, 0.7, and 1.0 V versus SCE, respectively. This is consistent with the formation of a strong oxidant (with a reversible potential higher than 1.0 V vs SCE), here assigned to the chlorine intermediate with a reversible potential of $E^\theta(\text{Cl}_2/\text{Cl}^-) = 1.115$ V versus SCE.²⁹

In addition to the pulses, it is possible to see a build-up of chlorine product (as an increase in the collector background reduction current with time) leading to about 80 nA current. Based on this, the apparent chlorine concentration in the solution phase in the immediate vicinity of the photoanode can be estimated³⁰ as $c = (I_{\text{lim}})/(4nFD\tau) = 4 \text{ mM}$ (only in the vicinity of the photoanode). Therefore, the formation of chlorine is evident, and the formation of hypochlorite (and chlorate) from chlorine is a follow-up chemical process that occurs over seconds to minutes in the bulk solution phase.

3.3. Photoelectrochemical Hypochlorite Formation III:

Kinetic Analysis. Impedance analysis for electrodes in aqueous NaCl was carried out for as-deposited and annealed samples. Figure 5A shows data for the as-deposited film at 0.4 V versus SCE applied potential under dark and illuminated conditions (blue LED, $\lambda = 405 \text{ nm}$). A change in phase angle at about 2 kHz is indicative of the RC time constant of the ITO– WO_3 –electrolyte interface (effective charging of the ITO electrode occurs only at lower frequencies).

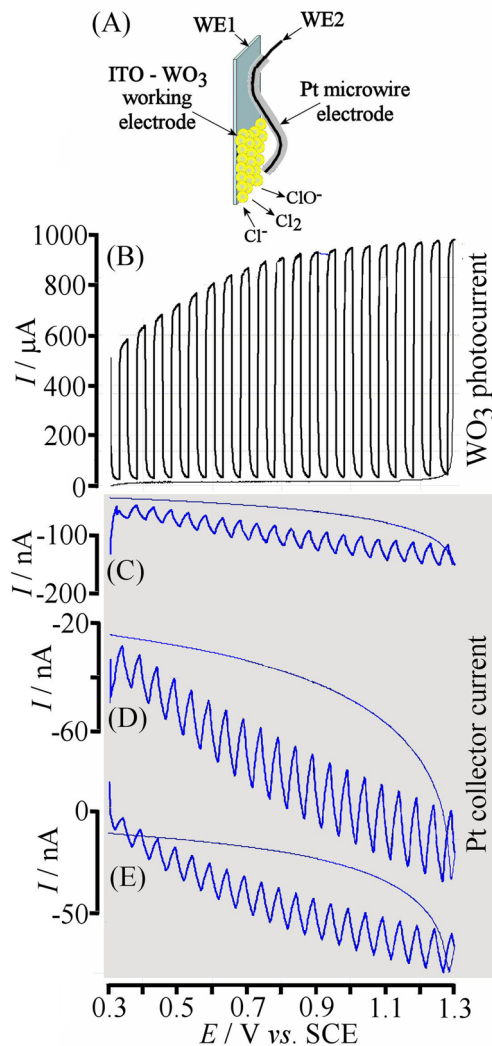


Figure 4. (A) Schematic drawing of the generator–collector electrode arrangement with a 50 μm Pt wire detecting products in the vicinity of the WO_3 photoanode. (B) Cyclic voltammogram (10 mV s^{-1} , blue light pulses 0.2 Hz) for an annealed WO_3 film electrode in 3 M NaCl. (C, D, and E) The corresponding collector current responses at applied potentials of 0.3, 0.7, and 1.0 V vs SCE, respectively.

When comparing with the impedance data for the annealed electrode (see Figure 5B), a shift of the RC-time constant for charging of the ITO– WO_3 –electrolyte interface from 2000 to approximately 200 Hz is apparent, which is caused by an ITO resistance increase (due to high temperature annealing in air). The effect of the light on the absolute impedance data is commencing at about 2 Hz for both as-deposited and annealed electrode. The change in phase angle back to close to zero at very low frequencies is consistent with the processes being dominated by the rate of electrochemical conversion of chloride to chlorine and to hypochlorite.

To further explore transient responses which were observed in voltammetry experiments for both as-deposited and annealed samples under pulsed light conditions (vide supra), chronoamperometry investigations with higher time resolution (ca. 1 ms) were performed at different applied potentials. Figure 6A shows data for as-deposited (i–iii) and annealed (iv) electrodes immersed in 3 M NaCl. Characteristic “spikes” are observed for both light-on and light-off transients in particular for the as-deposited films.

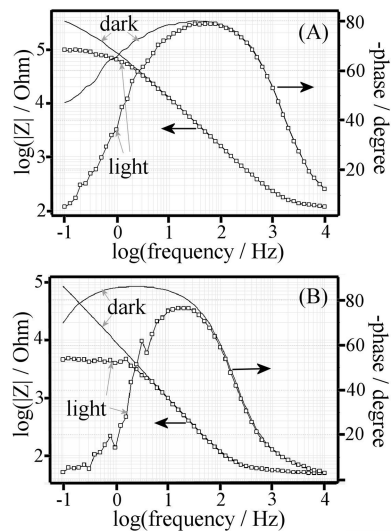


Figure 5. Impedance data for (A) as-deposited and (B) annealed nano-WO₃ films in 3 M NaCl at 0.4 V vs SCE (under light and dark conditions).

As-deposited film electrodes show a much stronger transient spike effect in particular at lower applied potentials. The “light-on” transient is associated with a short negative spike indicative of faster holes reaching the ITO electrode surface quickly (see scheme in Figure 6B). This is possible only in the first phase of illumination due to the corresponding build-up of electrons in the nano-WO₃ film (with increased recombination after build-up of a higher “electron” concentration) and the onset of the hole trapping by chloride leading to a net anodic photocurrent.

A lower mobility of electrons (or more correctly W(V) surface trap sites) is not surprising.

Once a photostationary state is reached (see Figure 6C), holes reacting with chloride lead to a net anodic photocurrent with electrons reaching the underlying ITO electrode surface. A gradient in the electron concentration with depletion toward the electrode surface is likely. The resulting effect of the gradient on the recombination rate also leads to a gradient in the hole concentration with effective hypochlorite formation most likely close to the ITO–WO₃ interface (but not so close that recombination through the ITO electrode dominates).

The “light-off” transient is again associated with a current spike, this time due to the excess electrons (see Figure 6D) that are present during the photostationary state. The spike “decay time” for light-on and for light-off transients appears similar (and potential dependent) which is indicative of a coupled diffusion process (hole and electron diffusion gradients coupled by recombination). The tentatively proposed mechanism chosen here may be contrasted to the single crystal semiconductor model and the build-up of charges within the bulk semiconductor material.³¹ Here, the weaker link between nanoparticles makes interparticle hole/electron hopping a surface process rather than a bulk process.

It is possible (and instructive) to reproduce the photo-transient results qualitatively with the help of an approximate 1D (homogeneous, 400 boxes, $\Delta t = 1 \mu\text{s}$) finite difference calculation³² based on eq 5.³³

$$\frac{\partial n_e}{\partial t} = \alpha I_{\text{ce}} e^{-\alpha x} + D_e \frac{\partial^2 n_e}{\partial x^2} - k_r n_e n_h \quad (5A)$$

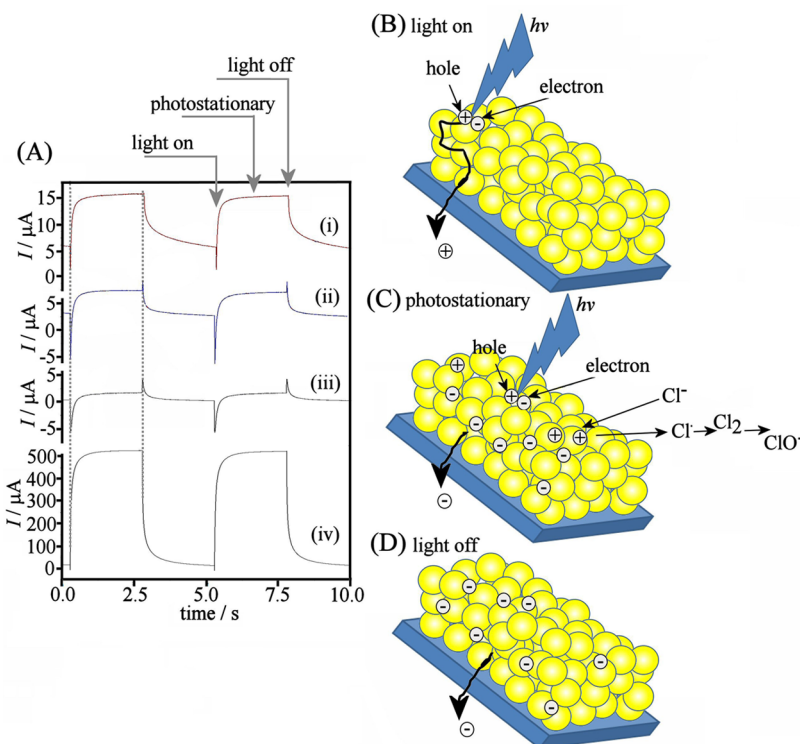


Figure 6. (A) Chronoamperometric data under pulsed light conditions (0.2 Hz) obtained in 3 M NaCl for the “as-deposited” electrode at (i) 0.8 V, (ii) 0.5 V, and (iii) 0.2 V vs SCE and (iv) for the “annealed” electrode at 0.5 V vs SCE. Also shown are schematic drawings of the mechanism under (B) light-on, (C) photostationary, and (D) light-off conditions.

$$\frac{\partial n_h}{\partial t} = \alpha I_o e^{-\alpha x} + D_e \frac{\partial^2 n_h}{\partial x^2} - k_r n_e n_h - k_c n_h \quad (5B)$$

In this set of equations, the concentration of electrons n_e and holes n_h are linked to the light intensity I_o , extinction coefficient α , diffusion coefficients D_e and D_h , bimolecular recombination rate constant k_r , and the chemical rate constant k_c for chlorine formation. Assuming a relatively slow rate of electron hopping, $D_e = 1 \times 10^{-14} \text{ m}^2 \text{ s}^{-1}$, and a 1 order of magnitude faster hole transport, $D_h = 3 \times 10^{-13} \text{ m}^2 \text{ s}^{-1}$, adjusting α to give about 90% absorption over 2 μm (SE configuration), and selecting $k_r = 5 \times 10^6 \text{ mol}^{-1} \text{ m}^3 \text{ s}^{-1}$ and $k_c = 50 \text{ s}^{-1}$ allows the transients shown in Figure 7A–C to be calculated. As a boundary condition, fully

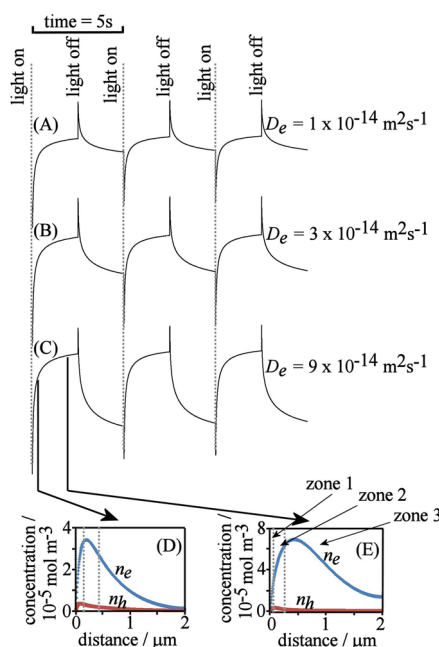


Figure 7. Simulated SE phototransients for (A) $D_e = 1 \times 10^{-14} \text{ m}^2 \text{ s}^{-1}$, (B) $D_e = 3 \times 10^{-14} \text{ m}^2 \text{ s}^{-1}$, and (C) $D_e = 9 \times 10^{-14} \text{ m}^2 \text{ s}^{-1}$ and a 1 order of magnitude faster hole transport $D_h = 3 \times 10^{-13} \text{ m}^2 \text{ s}^{-1}$, $k_r = 5 \times 10^6 \text{ mol}^{-1} \text{ m}^3 \text{ s}^{-1}$, and $k_c = 50 \text{ s}^{-1}$. (D) Plot of electron and hole concentrations n_e and n_h at time 0.2 s. (E) Plot of electron and hole concentrations n_e and n_h at time = 2.0 s.

reversible interfacial electron/hole transfer and instant recombination of holes and electrons in the substrate ITO electrode are assumed.

Varying the D_e parameter causes an apparent sharpening of the spikes for light-on and light-off transients (compare Figure 5A), although the overall relaxation rate appears similar. The main effect is an increase in the photostationary current with increased D_e . This is explained in the concentration gradient plots (see Figure 7D,E). A zone close to the electrode surface shows a diffusional gradient associated with the current into the electrode (diffusion zone increasing with time, zone 1), and a region far from the electrode is dominated by exponential decay of the light absorption (absorption zone, zone 3). Most interesting is the intermediate region (reaction zone, zone 2) where an imbalance of n_e and n_h exists and, in particular, close to the electrode where n_h is most significant (zone of high chlorine generation).

It is interesting to compare the experimental photocurrent transients at “annealed” and at “as-deposited” nano-WO₃ film electrodes. Transient peaks for light-on and light-off are much

less obvious [see Figure 6A(iv)]. This is likely to be due to (i) the higher photocurrent in the photostationary state masking the transients and (ii) shorter transients due to faster charge carrier mobility. The improved electrical contact between particles after annealing probably allows a more extended reaction zone for hole capture by chloride and a more active surface with smaller nanoparticles more effectively interconnected.

3.4. Photoelectrochemical Hypochlorite Formation IV: “Molecular Conduit” Effects.

The importance of charge carrier transport and recombination in photoinduced electrochemical processes appears crucial and it is possible to ask whether annealing is the only option to achieve improved electrical contact between nanoparticles (e.g., in printed films). Nanoparticle surface modification could be an option to achieve both improved electron conductivity and improved reactivity of holes with the aqueous phase. Surface modification of WO₃ films, for example, with Fe(III)³⁴ or Co²⁺³⁵ or modification of Fe₂O₃ with Co²⁺³⁶ has been reported to enhance the photoelectrochemical oxygen evolution process.

Here, the redox mediator approach is investigated. Cobalt(III) sepulchrate (see Figure 8B) is known as a versatile redox mediator^{37,38} with the ability to electron-transfer quench photoexcited states, for example, for Ru(bipy)₃^{2+*}.³⁷ The reversible potential has been reported at about -0.68 V versus SCE.³⁹ When the “as-deposited” nano-WO₃ film electrode is immersed in 1 mM Co(sep)³⁺ solution, rinsed, and dried, a considerable increase in anodic photocurrent is registered (similar to the increase after annealing). The effect can be further enhanced by repeating the Co(sep)³⁺ adsorption and drying steps up to six times. A typical I–V curve for pulsed blue light activation is shown in Figure 8A. In the presence of the Co(sep)³⁺ adsorbed onto the WO₃ surface enhancements of typically 1 order of magnitude are observed. This effect does not occur for the “annealed” WO₃ films either because of a change in surface properties with annealing (less effective Co(sep)³⁺ adsorption) or due to the higher underlying electron mobility due to annealing. Therefore, surface-bound Co(sep)³⁺ as a “molecular conduit” for electrons could be a useful low-temperature alternative to the high-temperature annealing process.

Although relatively stable during one scan, the Co(sep)³⁺ effect is not permanent and a decay occurs over several minutes. The effect is renewed by further Co(sep)³⁺ adsorption cycles. It seems likely that leaching out of the water-soluble Co(sep)³⁺ is mainly responsible for the decay. In the future, improved molecular conduit architectures (lower water solubility and stronger adsorption to WO₃) could be employed to achieve a more permanent enhancement effect.

The mechanism for the photocurrent enhancement is likely to be based on a “molecular conduit” effect, whereby Co(sep)³⁺ is able to speed up interparticle electron conduction (see Figure 8B,C, but also Figure 7). Energetically, the reversible potential for the Co(sep)^{3+/2+} redox system is more negative compared to the WO₃ valence band (or the W(V) surface redox sites, vide supra). This poses a problem because only a small fraction of Co(sep)³⁺ can be reduced at a given time. A simple calculation assuming Nernstian conditions (based on the reversible potential for Co(sep)^{3+/2+} and the WO₃ conduction band energy at pH 7 at ca. -0.4 V vs SCE⁴⁰) suggests that only 1 in 10⁵ molecules can be reduced at a given time, but non-Nernstian conditions at the WO₃ surface may significantly affect this number.

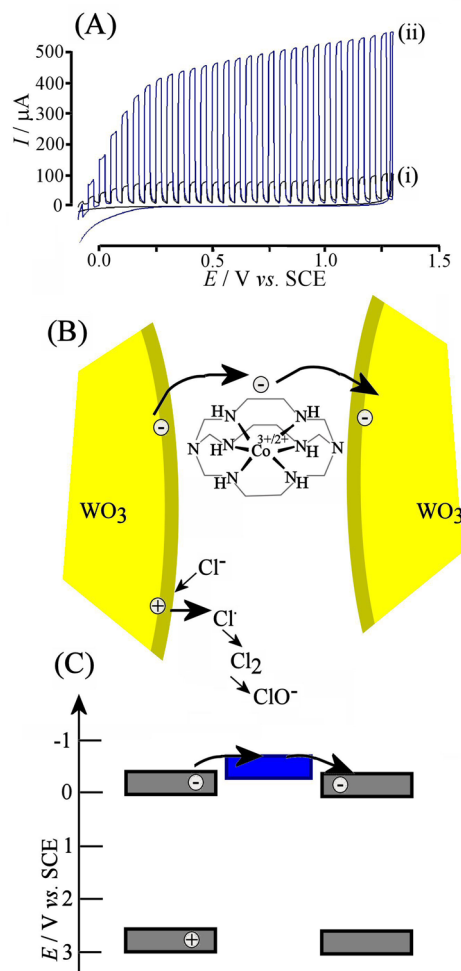


Figure 8. (A) Typical light-on–light-off transients (scan rate 10 mVs^{-1}) for an as-deposited nano- WO_3 film electrode immersed in 3 M NaCl. The effect of (i) no $\text{Co}(\text{sep})^{3+}$ adsorption and (ii) three $\text{Co}(\text{sep})^{3+}$ adsorption cycles is demonstrated. (B) Schematic drawing of $\text{Co}(\text{sep})^{3+}$ bridging two WO_3 nanoparticles. (C) Schematic energy level diagram for a $\text{Co}(\text{sep})^{3+}$ “molecular valence band conduit” between two WO_3 nanoparticles.

The relatively low level of $\text{Co}(\text{sep})^{2+}$ during irradiation may also be regarded as beneficial to avoid “draining” of electrons into the $\text{Co}(\text{sep})^{3+/2+}$ system, which could again increase recombination. The danger of enhanced recombination appears to be less important in this case and further improvements in molecular conduit architecture should be possible in future.

The ability to design a nanostructured material based on WO_3 that is deposited in a room temperature “roll-on” process without the need of high-temperature processing could be useful in the fabrication of practical devices on polymer supports with applications in solar energy harvesting and seawater photoelectrolysis.

4. CONCLUSIONS

It has been shown that nano- WO_3 applied to ITO electrode substrates in a “roll-on” process is active in the conversion of chloride to chlorine and hypochlorite. The as-deposited films are not as effective as the 500 °C annealed film electrodes. The reason for this is suggested to be predominantly lower electron/hole mobility (poor electrical contact between nanoparticles), but remaining *n*-hexanol capping the nano-

particle surface cannot be ruled out at this stage. A qualitative model based on charge carrier surface mobility (in contrast to bulk mobility) has been proposed. Based on this model, a reaction zone effect is inferred with a variation of the rate of chlorine production with distance from the substrate electrode. Very interesting is the effect of the $\text{Co}(\text{sep})^{3+}$ redox mediator adsorbed onto the WO_3 surface. For as-deposited films, photocurrent enhancements of an order of magnitude are observed and this effect is explained with a “molecular conduit” effect with the $\text{Co}(\text{sep})^{3+/2+}$ redox system, allowing hopping of electrons from particle to particle without “draining”. In the future, the design of appropriately stable and active molecular conduit architectures could help enhance photoelectrolysis processes. More quantitative models of charge carrier surface mobility and reactivity in mesoporous nanoparticle networks need to be developed.

■ AUTHOR INFORMATION

Corresponding Author

*Tel.: 01225383694. Fax: 01225386231. E-mail: f.marken@bath.ac.uk.

Notes

The authors declare no competing financial interest.

■ ACKNOWLEDGMENTS

S.A. thanks the HEC, Pakistan, for financial support. I.A.I.H. thanks the Egyptian government for a stipend. We are grateful for support and discussions with Professor L. M. Peter.

■ REFERENCES

- Rassaei, L.; Herrmann, M.; Gordeev, S. N.; Marken, F. Inter-Particle Charge Transfer in TiO_2 -phytate Films: Generator-Collector Gold–Gold Junction Transients. *J. Electroanal. Chem.* **2012**, *686*, 32–37.
- Tacca, A.; Meda, L.; Marra, G.; Savoini, A.; Caramori, S.; Cristino, V.; Bignozzi, C. A.; Pedro, V. G.; Boix, P. P.; Gimenez, S.; et al. Photoanodes Based on Nanostructured WO_3 for Water Splitting. *ChemPhysChem* **2012**, *13*, 3025–3034.
- Chen, Q. P.; Li, J. H.; Zhou, B. X.; Long, M. C.; Chen, H. C.; Liu, Y. B.; Cai, W. M.; Shangguan, W. F. Preparation of Well-Aligned WO_3 Nanoflake Arrays Vertically Grown on Tungsten Substrate as Photoanode for Photoelectrochemical Water Splitting. *Electrochim. Commun.* **2012**, *20*, 153–156.
- Scott-Emuakpor, E. O.; Kruth, A.; Todd, M. J.; Raab, A.; Paton, G. I.; Macphee, D. E. Remediation of 2,4-Dichlorophenol Contaminated Water by Visible Light-Enhanced WO_3 Photoelectrocatalysis. *Appl. Catal., B* **2012**, *123*, 433–439.
- Santato, C.; Ullmann, M.; Augustynski, J. Enhanced Visible Light Conversion Efficiency Using Nanocrystalline WO_3 Films. *Adv. Mater.* **2001**, *13*, 511–512.
- Caramori, S.; Cristino, V.; Meda, L.; Tacca, A.; Argazzi, R.; Bignozzi, C. A. Efficient Anodically Grown WO_3 for Photo-electrochemical Water Splitting. *EMRS Symp. T* **2012**, *22*, 127–136.
- Kwong, W. L.; Savvides, N.; Sorrell, C. C. Electrodeposited Nanostructured WO_3 Thin Films for Photoelectrochemical Applications. *Electrochim. Acta* **2012**, *75*, 371–380.
- Zheng, H. D.; Ou, J. Z.; Strano, M. S.; Kaner, R. B.; Mitchell, A.; Kalantar-Zadeh, K. Nanostructured Tungsten Oxide - Properties, Synthesis, and Applications. *Adv. Funct. Mater.* **2011**, *21*, 2175–2196.
- Gaikwad, N. S.; Waldner, G.; Bruger, A.; Belaidi, A.; Chaqour, S. M.; Neumann-Spallart, M. Photoelectrochemical Characterization of Semitransparent WO_3 Films. *J. Electrochem. Soc.* **2005**, *152*, G411–G416.
- Meda, L.; Tozzola, G.; Tacca, A.; Marra, G.; Caramori, S.; Cristino, V.; Bignozzi, C. A. Photo-electrochemical Properties of

- Nanostructured WO_3 Prepared with Different Organic Dispersing Agents. *Sol. Energy Mater. Sol. Cells* **2010**, *94*, 788–796.
- (11) Pesci, F. M.; Cowan, A. J.; Alexander, B. D.; Durrant, J. R.; Klug, D. R. Charge Carrier Dynamics on Mesoporous WO_3 During Water Splitting. *J. Phys. Chem. Lett.* **2011**, *2*, 1900–1903.
- (12) Janaky, C.; Rajeshwar, K.; de Tacconi, N. R.; Chanmanee, W.; Huda, M. N. Tungsten-Based Oxide Semiconductors for Solar Hydrogen Generation. *Catal. Today* **2013**, *199*, 53–64.
- (13) Wang, J. M.; Sun, X. W.; Jiao, Z. H. Application of Nanostructures in Electrochromic Materials and Devices: Recent Progress. *Materials* **2010**, *3*, 5029–5053.
- (14) Deepa, M.; Srivastava, A. K.; Saxena, T. K.; Agnihotry, S. A. Annealing Induced Microstructural Evolution of Electrodeposited Electrochromic Tungsten Oxide Films. *Appl. Surf. Sci.* **2005**, *252*, 1568–1580.
- (15) Xin, G.; Guo, W.; Ma, T. L. Effect of Annealing Temperature on the Photocatalytic Activity of WO_3 for O_2 Evolution. *Appl. Surf. Sci.* **2009**, *256*, 165–169.
- (16) Penner, S.; Liu, X.; Klotzer, B.; Klauser, F.; Jenewein, B.; Bertel, E. The Structure and Composition of Oxidized and Reduced Tungsten Oxide Thin Films. *Thin Solid Films* **2008**, *516*, 2829–2836.
- (17) Liu, X.; Wang, F. Y.; Wang, Q. Nanostructure-Based WO_3 Photoanodes for Photoelectrochemical Water Splitting. *Phys. Chem. Chem. Phys.* **2012**, *14*, 7894–7911.
- (18) Augustynski, J.; Solarska, R.; Hagemann, H.; Santato, C. Nanostructured Thin-Film Tungsten Trioxide Photoanodes for Solar Water and Sea-Water Splitting. *Sol. Hydrogen Nanotechnol.* **2006**, *6340*, U140–U148.
- (19) Alexander, B. D.; Kulesza, P. J.; Rutkowska, L.; Solarska, R.; Augustynski, J. Metal Oxide Photoanodes for Solar Hydrogen Production. *J. Mater. Chem.* **2008**, *18*, 2298–2303.
- (20) Hill, J. C.; Choi, K. S. Effect of Electrolytes on the Selectivity and Stability of *n*-type WO_3 Photoelectrodes for Use in Solar Water Oxidation. *J. Phys. Chem. C* **2012**, *116*, 7612–7620.
- (21) Solarska, R.; Santato, C.; Jorand-Sartoretti, C.; Ulmann, M.; Augustynski, J. Photoelectrolytic Oxidation of Organic Species at Mesoporous Tungsten Trioxide Film Electrodes under Visible Light Illumination. *J. Appl. Electrochem.* **2005**, *35*, 715–721.
- (22) Yang, B.; Barnes, P. R. F.; Zhang, Y.; Luca, V. Tungsten Trioxide Films with Controlled Morphology and Strong Photocatalytic Activity via a Simple Sol-Gel Route. *Catal. Lett.* **2007**, *118*, 280–284.
- (23) Reyes, L. F.; Saukko, S.; Hoel, A.; Lantto, V.; Granqvist, C. G.; Lappalainen, J. Improved Gas Response at Room Temperature of Activated Nanocrystalline WO_3 Films. *Phys. Scr.* **2004**, *T114*, 240–243.
- (24) Fraga, L. E.; Anderson, M. A.; Beatriz, M.L.P.M.A.; Paschoal, F. M. M.; Romao, L. P.; Zanoni, M. V. B. Evaluation of the Photoelectrocatalytic Method for Oxidizing Chloride and Simultaneous Removal of MicrocystinToxins in Surface Waters. *Electrochim. Acta* **2009**, *54*, 2069–2076.
- (25) Soliman, H. M. A.; Kashyout, A. B.; El Nouby, M. S.; Abosehly, A. M. Preparation and Characterizations of Tungsten Oxide Electrochromic Nanomaterials. *J. Mater. Sci.: Mater. Electron.* **2010**, *21*, 1313–1321.
- (26) Bamwenda, G. R.; Arakawa, H. The Visible Light Induced Photocatalytic Activity of Tungsten Trioxide Powders. *Appl. Catal., A* **2001**, *210*, 181–191.
- (27) Zanoni, M. V. B.; Sene, J. J.; Selcuk, H.; Anderson, M. A. Photoelectrocatalytic Production of Active Chlorine on Nanocrystalline Titanium Dioxide Thin-Film Electrodes. *Environ. Sci. Technol.* **2004**, *38*, 3203–3208.
- (28) Gondal, M. A.; Dastageer, M. A.; Khalil, A. Synthesis of Nano- WO_3 and its Catalytic Activity for Enhanced Antimicrobial Process for Water Purification Using Laser Induced Photo-catalysis. *Catal. Commun.* **2009**, *11*, 214–219.
- (29) Bard, A. J.; Parsons, R.; Jordan, J. *Standard Potentials in Aqueous Solution*; Marcel Dekker: New York, 1985; p 71.
- (30) Oldham, K. B.; Myland, J. C.; Bond, A. M. *Electrochemical Science and Technology*; Wiley: Toronto, 2012; p 247.
- (31) Peter, L. M. Energetics and Kinetics of Light-Driven Oxygen Evolution at Semiconductor Electrodes: The Example of Hematite. *J. Solid State Electrochem.* **2013**, *17*, 315–326.
- (32) Bard, A. J.; Faulkner, L. R. *Electrochemical Methods*; Wiley: New York, 2001; p 785.
- (33) Peter, L. M.; Wijayantha, K.G.U Electron Transport and Back Reaction in Dye Sensitised Nanocrystalline Photovoltaic Cells. *Electrochim. Acta* **2000**, *45*, 4543–4551.
- (34) Han, S.; Li, J.; Chen, X.; Huang, Y.; Liu, C. J.; Yang, Y. H.; Li, W. Z. Enhancing Photoelectrochemical Activity of Nanocrystalline WO_3 Electrodes by Surface Tuning with Fe(III). *Int. J. Hydrogen Energy* **2012**, *37*, 16810–16816.
- (35) Seabold, J. A.; Choi, K. S. Effect of a Cobalt-Based Oxygen Evolution Catalyst on the Stability and the Selectivity of Photo-Oxidation Reactions of a WO_3 Photoanode. *Chem. Mater.* **2011**, *23*, 1105–1112.
- (36) Cummings, C. Y.; Marken, F.; Peter, L. M.; Tahir, A. A.; Wijayantha, K. G. U. Kinetics and Mechanism of Light-Driven Oxygen Evolution at Thin Film $\alpha\text{-Fe}_2\text{O}_3$ Electrodes. *Chem. Commun.* **2012**, *48*, 2027–2029.
- (37) Scandola, M.; Scandola, F.; Indelli, A.; Balzani, V. Cobalt(III) Sepulchrate—A New Relay for Water Splitting Photochemical Cycles. *Inorg. Chim. Acta, Lett.* **1983**, *76*, L67–L68.
- (38) Creaser, I. I.; Harrowfield, J. M.; Herlt, A. J.; Sargeson, A. M.; Spingborg, J.; Geue, R. J.; Snow, M. R. Sepulchrate - Macrobicyclic Nitrogen Cage for Metal Ions. *J. Am. Chem. Soc.* **1977**, *99*, 3181–3182.
- (39) Cekic, S. Z.; Holtmann, D.; Guven, G.; Mangold, K. M.; Schwaneberg, U.; Schrader, J. Mediated Electron Transfer with P450cin. *Electrochim. Commun.* **2010**, *12*, 1547–1505.
- (40) Djellal, L.; Bellal, B.; Trari, M. Physical, Photoelectrochemical Properties of CuIn_3Se_5 and Relevance for Hydrogen Production. *Mater. Chem. Phys.* **2012**, *137*, 340–345.